JCTC Journal of Chemical Theory and Computation

Electronic Structure Calculations under Periodic Boundary Conditions Based on the Gaussian and Fourier Transform (GFT) Method

Tomomi Shimazaki* and Yoshihiro Asai

National Institute of Advanced Industrial Science and Technology (AIST), Umezono 1-1-1, Tsukuba Central 2, Tsukuba, Ibaraki 305-8568, Japan

Received August 12, 2008

Abstract: We developed the Gaussian and Fourier transform method for crystalline systems. In this method, the Hartree (Coulomb) term of valence electron contribution is taken into account by solving the Poisson equation based on Fourier transform technique. We compared the band structures obtained by the Hartee-Fock (HF) approximation and the density functional theory (DFT). We used three different types of density functional approximations such as the local density approximation (LDA), generalized gradient approximation (GGA), and hybrid density functional. In this paper, we confirm that our calculation technique yields similar results to previous studies.

I. Introduction

The crystal orbital (CO) method based on the Gaussian basis set has been developed for first-principle calculations under the periodic boundary condition (PBC),[1−9] where the direct lattice sum of the Hartree term is the most time-consuming part of the calculation due to the slow decay of the Coulomb potential. The cutoff technique[10] and the fast multipole method (FMM)[5,11−14] have been used for resolving this problem. In this paper, we employ the Fourier transform for calculating the Hartree term. The Fourier transform technique provides an exact solution for the Hartree term under the periodic boundary conditions, and therefore this feature is a major advantage for band calculations in crystalline systems. In our technique, the direct lattice sum calculation based on the Gaussian basis set is used for determining the "core" Hartree (Coulomb) term employed to describe the core electrons. We also discuss the effective core potential (ECP) technique for the "core" term in this paper. On the other hand, the electron density of the valence electrons is represented by the auxiliary plane wave basis set, and the Poisson equation is solved by using the Fourier transform (FT) in order to obtain the "valence" Hartree (Coulomb) term. Therefore, we refer to our technique as the Gaussian and Fourier Transform (GFT) method in this paper. It should be noted that while the GFT method is similar to previous studies, its details are different. For example, Lippert et al. reported the Gaussian and augmented plane wave (GAPW) method,[15,16] in which both the Gaussian function and the plane wave are used as representations of the valence electron density, and the core electrons are eliminated by introducing atomic pseudopotentials. Moreover, Krack et al. extended the GAPW method to all-electron calculations.[17] The GPW method, which is a sister version of the GAPW method, was reported by VandeVondele et al.,[18] and Füsti-Molnár et al. adopted an the auxiliary plane wave technique in the Fourier transform Coulomb (FTC) method.[19] In addition, Kurashige et al. reported the adaptive density portioning technique (ADPT) for efficient Fourier transform calculations.[20] Other techniques for large molecular systems have been reported.[21−24] On the other hand, Wieferink et al. employed the Gaussian function and the Fourier transform in order to obtain the k-dependent energy band structure,[25,26] and some applications have been reported.[27,28] While they used pseudopotentials, in this paper we show not only the use of effective core potential but also an explicit treatment of core electrons. In the following section, we explain the details of the GFT method. In Section III, we show the energy band structure of diamond obtained with our method and compare those results with previous studies, and a summary is presented in Section V.

* Corresponding author e-mail: t-shimazaki@aist.go.jp.

10.1021/ct800329m CCC: $40.75
Published on Web 11/25/2008

II. Theory

A. Gaussian and Fourier Transform (GFT) Method. In this section, we explain the GFT method for crystalline systems. The Bloch function (crystal orbital) is defined as the linear combination of atomic orbitals (LCAO) expansion as follows[1,2]

$$b_j^{\mathbf{k}}(\mathbf{r}) = \frac{1}{\sqrt{K}} \sum_{\alpha}^{M} \sum_{\mathbf{Q}}^{K} \exp(i\mathbf{k}\cdot\mathbf{Q}) d_{\alpha,j}^{\mathbf{k}}(\mathbf{k}) \chi_{\alpha}^{\mathbf{Q}} \tag{1}$$

where $\mathbf{Q}$ is the translation vector. The total number of cells is $K = K_1K_2K_3$, where K_1, K_2, and K_3 are the number of cells in the direction of each crystal axis, and $\mathbf{k}$ is the wave vector. $\chi_{\alpha}^{\mathbf{Q}} = \chi_{\alpha}(\mathbf{r} - \mathbf{Q} - \mathbf{r}_{\alpha})$ is the α-th atomic orbital (AO), whose center is displaced from the origin of the unit cell at $\mathbf{Q}$ by $\mathbf{r}_{\alpha}$. In this paper, we use Greek letters to indicate the indexes of the atomic orbitals. $d_{\alpha,j}^{\mathbf{k}}$ is the LCAO coefficient, which is obtained from the following Schrödinger equation, and j is the suffix for the molecular orbital (MO).

$$\mathbf{h}(\mathbf{k})\mathbf{d}_j^{\mathbf{k}} = \lambda_j^{\mathbf{k}} \mathbf{S}(\mathbf{k})\mathbf{d}_j^{\mathbf{k}} \tag{2-1}$$

$$\mathbf{d}_j^{\mathbf{k}} = (d_{1,j}^{\mathbf{k}} \quad d_{2,j}^{\mathbf{k}} \quad \cdots \quad d_{\alpha,j}^{\mathbf{k}} \quad \cdots \quad d_{M,j}^{\mathbf{k}})^T \tag{2-2}$$

$$\mathbf{h}(\mathbf{k}) = \sum_{\mathbf{Q}}^{K} \exp(i\mathbf{k}\cdot\mathbf{Q})\mathbf{h}(\mathbf{Q}) \tag{2-3}$$

$$\mathbf{S}(\mathbf{k}) = \sum_{\mathbf{Q}}^{K} \exp(i\mathbf{k}\cdot\mathbf{Q})\mathbf{S}(\mathbf{Q}) \tag{2-4}$$

$$\mathbf{d}_j^{\mathbf{k}*T}\mathbf{S}(\mathbf{k})\mathbf{d}_{j'}^{\mathbf{k}} = \delta_{j,j'} \tag{2-5}$$

Here, the Hamiltonian and the overlap matrices are given by $[\mathbf{h}(\mathbf{Q})]_{\alpha\beta} = \langle \chi_{\alpha}^{\mathbf{Q}_1} | \hat{h} | \chi_{\beta}^{\mathbf{Q}_2} \rangle$ and $[\mathbf{S}(\mathbf{Q})]_{\alpha\beta} = \langle \chi_{\alpha}^{\mathbf{Q}_1} | \chi_{\beta}^{\mathbf{Q}_2} \rangle$, respectively. $\hat{h}$ is the one-electron Hamiltonian operator, and $\mathbf{Q} = \mathbf{Q}_2 - \mathbf{Q}_1$. The Bloch functions satisfy the following orthonormal relation, $\langle b_{j'}^{\mathbf{k}'}(\mathbf{r}) | b_j^{\mathbf{k}}(\mathbf{r}) \rangle = \delta_{\mathbf{k}',\mathbf{k}}\delta_{j',j}$.

The one-electron Hamiltonian matrix is composed of the following terms.

$$\mathbf{h}(\mathbf{Q}) = \mathbf{T}(\mathbf{Q}) + \mathbf{V}_{NA}(\mathbf{Q}) + \mathbf{V}_{Hartree}(\mathbf{Q}) + \mathbf{V}_{XC}(\mathbf{Q}) \tag{3}$$

Here, $\mathbf{T}(\mathbf{Q})$ represents the kinetic term, whose matrix element is obtained from $[\mathbf{T}(\mathbf{Q})]_{\alpha\beta} = \langle \chi_{\alpha}^{\mathbf{0}} | -(1/2)\nabla^2 | \chi_{\beta}^{\mathbf{Q}} \rangle$. $\mathbf{V}_{NA}(\mathbf{Q})$ is the nuclear attraction term, $\mathbf{V}_{Hartree}(\mathbf{Q})$ is the Hartree term, and $\mathbf{V}_{XC}(\mathbf{Q})$ is the exchange correlation term. In this paper, we divided $\mathbf{V}_{NA}(\mathbf{Q}) + \mathbf{V}_{Hartree}(\mathbf{Q})$ into core and valence contributions as follows.

$$\mathbf{V}_{NA}(\mathbf{Q}) + \mathbf{V}_{Hartree}(\mathbf{Q}) = \mathbf{V}_{NA}^{core}(\mathbf{Q}) + \mathbf{V}_{Hartree}^{core}(\mathbf{Q}) + \mathbf{V}_{SR-NA}^{valence}(\mathbf{Q}) + \mathbf{V}_{LR-NA}^{valence}(\mathbf{Q}) + \mathbf{V}_{Hartree}^{valence}(\mathbf{Q}) \tag{4}$$

The above equation is obtained by simply dividing the terms into core and valence contributions, where $\mathbf{V}_{NA}^{core}(\mathbf{Q})$ and $\mathbf{V}_{Hartree}^{core}(\mathbf{Q})$ are the nuclear attraction and Hartree terms for the core contribution, respectively. $\mathbf{V}_{SR-NA}^{valence}(\mathbf{Q})$ and $\mathbf{V}_{LR-NA}^{valence}(\mathbf{Q})$ are the short-range (SR) and long-range (LR) nuclear attraction terms, respectively, for the valence contribution. $\mathbf{V}_{Hartree}^{valence}(\mathbf{Q})$ is the Hartree term for the valence contribution. We will discuss the details of these terms later. The division into core and valence contributions is an essential concept in the GFT method. In this method, two different techniques are adopted for calculating the Coulomb interactions. The electron−electron and electron−nuclear interactions of the core contribution are directly determined based on the conventional quantum chemical (direct lattice sum) calculations. We will discuss the GFT method together with the effective core potential (ECP) in the next section. On the other hand, the interactions of valence contribution are considered by using the Poisson equation and the Fourier transform. The core electrons are strongly localized, and the direct lattice sum calculation is therefore more suitable. If we apply the Fourier transform to the core contribution, many plane waves are required. On the other hand, the lattice sum calculation for the valence contribution requires excessively long CPU times due to the long-range behavior of the Coulomb interactions. Therefore, the Fourier transform approach is more efficient for valence contribution, whereas the GFT method gives the exact solution for long-range Coulomb interactions. In other words, each of these two different techniques compensates for disadvantages of the other one.

In order to divide the terms into core and valence contributions, we introduce the following core and valence electron densities.

$$\rho(\mathbf{r}) = \sum_{\alpha}\sum_{\beta}\sum_{\mathbf{Q}_1,\mathbf{Q}_2} \mathbf{D}_{\alpha\beta}(\mathbf{Q}_2 - \mathbf{Q}_1)\chi_{\beta}^{\mathbf{Q}_2}(\mathbf{r})\chi_{\alpha}^{\mathbf{Q}_1}(\mathbf{r}) = \sum_{\alpha}\sum_{\beta}\sum_{\mathbf{Q}_1,\mathbf{Q}_3} \mathbf{D}_{\alpha\beta}(\mathbf{Q}_3)\chi_{\alpha}^{\mathbf{Q}_1}(\mathbf{r})\chi_{\beta}^{\mathbf{Q}_1+\mathbf{Q}_3}(\mathbf{r}) = \rho^{core}(\mathbf{r}) + \rho^{valence}(\mathbf{r}) \tag{5-1}$$

$$\rho^{core}(\mathbf{r}) = \sum_{\alpha}^{core}\sum_{\beta}^{core}\sum_{\mathbf{Q}_1,\mathbf{Q}_3} \mathbf{D}_{a\beta}(\mathbf{Q}_3)\chi_{\alpha}^{\mathbf{Q}_1}(\mathbf{r})\chi_{\beta}^{\mathbf{Q}_1+\mathbf{Q}_3}(\mathbf{r}) + \sum_{\alpha}^{core}\sum_{\beta}^{valence}\sum_{\mathbf{Q}_1,\mathbf{Q}_3} \mathbf{D}_{a\beta}(\mathbf{Q}_3)\chi_{\alpha}^{\mathbf{Q}_1}(\mathbf{r})\chi_{\beta}^{\mathbf{Q}_1+\mathbf{Q}_3}(\mathbf{r}) + \sum_{\alpha}^{valence}\sum_{\beta}^{core}\sum_{\mathbf{Q}_1,\mathbf{Q}_3} \mathbf{D}_{a\beta}(\mathbf{Q}_3)\chi_{\alpha}^{\mathbf{Q}_1}(\mathbf{r})\chi_{\beta}^{\mathbf{Q}_1+\mathbf{Q}_3}(\mathbf{r}) \tag{5-2}$$

$$\rho^{valence}(\mathbf{r}) = \sum_{\alpha}^{valence}\sum_{\beta}^{valence}\sum_{\mathbf{Q}_1,\mathbf{Q}_3} \mathbf{D}_{\alpha\beta}(\mathbf{Q}_3)\chi_{\alpha}^{\mathbf{Q}_1}(\mathbf{r})\chi_{\beta}^{\mathbf{Q}_1+\mathbf{Q}_3}(\mathbf{r}) \tag{5-3}$$

Here, $\rho(\mathbf{r})$ is the total electron density, and $\rho^{core}(\mathbf{r})$ and $\rho^{valence}(\mathbf{r})$ are the core and valence electron densities, respectively. The density matrix is obtained from the following equation

$$\mathbf{D}_{\alpha\beta}(\mathbf{Q}) = \frac{1}{K}\sum_{\mathbf{k}}\sum_{j} f_{FD}(E_F - \lambda_j^{\mathbf{k}}) d_{\alpha,j}^{\mathbf{k}*} d_{\beta,j}^{\mathbf{k}} \exp(i\mathbf{k}\cdot\mathbf{Q}) \tag{6}$$

where $f_{FD}(E_F - \lambda_j^{\mathbf{k}})$ and E_F are the Fermi-Dirac distribution function and the Fermi energy, respectively. The Hartree potential is divided into core and valence contributions on the basis of eqs (5-1), (5-2), and (5-3) as follows.

$$V_{Hartree}(\mathbf{r}) = \int \frac{\rho(\mathbf{r}')}{|\mathbf{r} - \mathbf{r}'|} d\mathbf{r}' = \int \frac{\rho^{core}(\mathbf{r}')}{|\mathbf{r} - \mathbf{r}'|} d\mathbf{r}' + \int \frac{\rho^{valence}(\mathbf{r}')}{|\mathbf{r} - \mathbf{r}'|} d\mathbf{r}' \equiv V_{Hartree}^{core}(\mathbf{r}) + V_{Hartree}^{valence}(\mathbf{r}) \tag{7}$$

The "core" Hartree term for crystalline systems is determined from the "core" contribution of the density matrix as follows

$$[\mathbf{V}^{core}_{Hartree}(\mathbf{Q})]_{\alpha\beta} = \langle\chi^{\mathbf{0}}_{\alpha}|V^{core}_{Hartree}|\chi^{\mathbf{Q}}_{\beta}\rangle = \sum_{\gamma}^{core}\sum_{\delta}^{core}\sum_{\mathbf{Q}_1,\mathbf{Q}_2}\mathbf{D}_{\gamma\delta}(\mathbf{Q}_1-\mathbf{Q}_2)\langle\chi^{\mathbf{0}}_{\alpha}\chi^{\mathbf{Q}_1}_{\gamma}|\chi^{\mathbf{Q}}_{\beta}\chi^{\mathbf{Q}_2}_{\delta}\rangle + \sum_{\gamma}^{core}\sum_{\delta}^{valence}\sum_{\mathbf{Q}_1,\mathbf{Q}_2}\mathbf{D}_{\gamma\delta}(\mathbf{Q}_1-\mathbf{Q}_2)\langle\chi^{\mathbf{0}}_{\alpha}\chi^{\mathbf{Q}_1}_{\gamma}|\chi^{\mathbf{Q}}_{\beta}\chi^{\mathbf{Q}_2}_{\delta}\rangle + \sum_{\gamma}^{valence}\sum_{\delta}^{core}\sum_{\mathbf{Q}_1,\mathbf{Q}_2}\mathbf{D}_{\gamma\delta}(\mathbf{Q}_1-\mathbf{Q}_2)\langle\chi^{\mathbf{0}}_{\alpha}\chi^{\mathbf{Q}_1}_{\gamma}|\chi^{\mathbf{Q}}_{\beta}\chi^{\mathbf{Q}_2}_{\delta}\rangle \quad (8\text{-}1)$$

$$\langle\chi^{\mathbf{0}}_{\alpha}\chi^{\mathbf{Q}_1}_{\gamma}|\chi^{\mathbf{Q}}_{\beta}\chi^{\mathbf{Q}_2}_{\delta}\rangle = \int\int\chi^{\mathbf{0}}_{\alpha}(\mathbf{r}_1)\chi^{\mathbf{Q}}_{\beta}(\mathbf{r}_1)\frac{1}{r_{12}}\chi^{\mathbf{Q}_1}_{\gamma}(\mathbf{r}_2)\chi^{\mathbf{Q}_2}_{\delta}(\mathbf{r}_2)d\mathbf{r}_1d\mathbf{r}_2 \quad (8\text{-}2)$$

where $r_{12} = |\mathbf{r}_1 - \mathbf{r}_2|$. The lattice sum over a small number of sites is required since the core electrons are strongly localized around the center of the nucleus and their charges are thus perfectly compensated by the core nuclear charges. We will discuss the "valence" Hartree term later. The nuclear attractive potential is also divided into core and valence contributions as follows.

$$V_{NA}(\mathbf{r}) = \sum_A\frac{Z_A}{|\mathbf{r}-\mathbf{R}_A|} = \sum_A\frac{Z^{core}_A}{|\mathbf{r}-\mathbf{R}_A|} + \sum_A\frac{Z^{valence}_A}{|\mathbf{r}-\mathbf{R}_A|} \equiv V^{core}_{NA}(\mathbf{r}) + V^{valence}_{NA}(\mathbf{r}) \quad (9)$$

Here, Z_A is the nuclear charge for atom number A. The "core" nuclear charge Z^{core}_A is defined as follows.

$$Z^{core}_A = \sum_{\alpha\in A}^{core}\sum_{\beta}^{core}\sum_{\mathbf{Q}}\mathbf{D}_{a\beta}(\mathbf{Q})\mathbf{S}_{\beta a}(\mathbf{Q}) + \sum_{\alpha\in A}^{core}\sum_{\beta}^{valence}\sum_{\mathbf{Q}}\mathbf{D}_{a\beta}(\mathbf{Q})\mathbf{S}_{\beta a}(\mathbf{Q}) + \sum_{\alpha\in A}^{valence}\sum_{\beta}^{core}\sum_{\mathbf{Q}}\mathbf{D}_{a\beta}(\mathbf{Q})\mathbf{S}_{\beta a}(\mathbf{Q}) \quad (10)$$

The remaining charge is assigned as the "valence" nuclear charge $Z^{valence}_A$ as follows.

$$Z^{valence}_A = Z_A - Z^{core}_A \quad (11)$$

The "core" nuclear attraction term is obtained as follows.

$$[\mathbf{V}^{core}_{NA}(\mathbf{Q})]_{\alpha\beta} = -\langle\chi^{\mathbf{0}}_{\alpha}|V^{core}_{NA}|\chi^{\mathbf{Q}}_{\beta}\rangle = -\langle\chi^{\mathbf{0}}_{\alpha}|\sum_A\frac{Z^{core}_A}{|\mathbf{r}-\mathbf{R}_A|}|\chi^{\mathbf{Q}}_{\beta}\rangle \quad (12)$$

Note that the "core" and "valence" nuclear charges are renewed in each self-consistent field (SCF) cycle.

Next, we discuss the "valence" contribution of the nuclear attraction and the Hartree terms. In the GFT method, the "valence" nuclear attractive potential is divided into short-range (SL) and long-range (LR) contributions, where $V^{valence}_{NA} = V^{valence}_{SR-NA} + V^{valence}_{LR-NA}$. For that purpose, we adopt the following error function (erf) and complementary error function (erfc).

$$\frac{1}{r} = \frac{erf(wr)}{r} + \frac{erfc(wr)}{r} \quad (13\text{-}1)$$

$$erf(wr) = \int_0^{wr}\exp(-t^2)dt \quad (13\text{-}2)$$

The short-range (SR) "valence" nuclear attraction term is determined from the complementary error function (erfc) and the "valence" nuclear charges $Z^{valence}_A$ as follows.

$$[\mathbf{V}^{valence}_{SR-NA}(\mathbf{Q})]_{\alpha\beta} = -\langle\chi^{\mathbf{0}}_{\alpha}|V^{valence}_{SR-NA}|\chi^{\mathbf{Q}}_{\beta}\rangle = -\langle\chi^{\mathbf{0}}_{\alpha}|\sum_A\frac{Z^{valence}_A erfc(\sqrt{\eta}|\mathbf{r}-\mathbf{R}_A|)}{|\mathbf{r}-\mathbf{R}_A|}|\chi^{\mathbf{Q}}_{\beta}\rangle \quad (14)$$

It is also necessary to calculate the long-range (LR) nuclear attraction term corresponding to the valence nuclear charge, which is given by the error function, $Z^{valence}_A erf(\eta^{1/2}|\mathbf{r}-\mathbf{R}_A|)/|\mathbf{r}-\mathbf{R}_A|$. The term is considered together with the "valence" Hartree term, as seen below. The sum of the "valence" Hartree and the long-range "valence" nuclear attraction terms, i.e., $\mathbf{V}^{valence}_{LR-NA}(\mathbf{Q})+\mathbf{V}^{valence}_{Hartree}(\mathbf{Q})$, is obtained from the following Poisson equation.

$$[\mathbf{V}^{valence}_{Hartree}(\mathbf{Q}) + \mathbf{V}^{valence}_{LR-NA}(\mathbf{Q})]_{\alpha\beta} = \langle\chi^{\mathbf{0}}_{\alpha}|V^{valence}_{Hartree} + V^{valence}_{LR-NA}|\chi^{\mathbf{Q}}_{\beta}\rangle = \langle\chi^{\mathbf{0}}_{\alpha}|V_{PE}(\mathbf{r})|\chi^{\mathbf{Q}}_{\beta}\rangle = [\mathbf{V}_{PE}(\mathbf{Q})]_{\alpha\beta} \quad (15\text{-}1)$$

$$\nabla^2V_{PE}(\mathbf{r}) = -4\pi\left[-\rho^{valence}(\mathbf{r}) + \sum_A Z^{valence}_A\left(\frac{\eta}{\pi}\right)^{\frac{3}{2}}\times\exp(-\eta|\mathbf{r}-\mathbf{R}_A|^2)\right] \equiv -4\pi\rho^{valence}_{Total}(\mathbf{r}) \quad (15\text{-}2)$$

The first term in eq (15-2) corresponds to the valence electrons, and the second term corresponds to the valence nuclear charges. In order to obtain these equations, we used the relation, $-\nabla^2(erf(\eta^{1/2}r)/r) = 4\pi(\eta/\pi)^{3/2}\exp(-\eta r^2)$.

In the Hartree−Fock approximation, the Fock exchange term $\mathbf{V}_X(\mathbf{Q})$ is obtained as follows.

$$[\mathbf{V}^{Fock}_X(\mathbf{Q})]_{\alpha\beta} = -\sum_{\gamma}\sum_{\delta}\sum_{\mathbf{Q}_1,\mathbf{Q}_2}\mathbf{D}_{\gamma\delta}(\mathbf{Q}_1-\mathbf{Q}_2)\langle\chi^{\mathbf{0}}_{\alpha}\chi^{\mathbf{Q}}_{\beta}|\chi^{\mathbf{Q}_1}_{\gamma}\chi^{\mathbf{Q}_2}_{\delta}\rangle \quad (16)$$

It should be noted that the determination of the Fock exchange term may be the most time-consuming part when we employ a fast evaluation technique for the Hartree term, such as the Fourier transform method and the fast multipole method (FMM). Although Izmaylov et al. tackled this problem and proposed an efficient evaluation technique of short-range Fock exchange term,[7] we simply estimate the Fock exchange term by truncating the sum of eq (16) in this paper.

B. Effective Core Potential (ECP). When we employ the effective core potential (ECP) together with the GFT method, the core electron density, $\rho^{core}(\mathbf{r})$, and nuclear charges, Z^{core}_A, become zero, and the ECP term, $\mathbf{V}_{ECP}$, is replaced instead of $\mathbf{V}^{core}_{Hartree} + \mathbf{V}^{core}_{NA}$ as follows.

$$\mathbf{h}(\mathbf{Q}) = \mathbf{T}(\mathbf{Q}) + \mathbf{V}_{ECP}(\mathbf{Q}) + \mathbf{V}^{valence}_{NA-SR}(\mathbf{Q}) + \mathbf{V}^{valence}_{NA-LR}(\mathbf{Q}) + \mathbf{V}^{valence}_{Hartree}(\mathbf{Q}) + \mathbf{V}_{XC}(\mathbf{Q}) \quad (17)$$

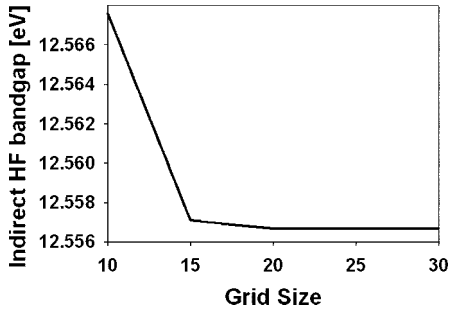

Figure 1. Changes of the indirect HF energy band gap with respect to the FFT grid size. The number of horizontal axis indicates the $N \times N \times N$ FFT grid. In this paper, we employ the $25 \times 25 \times 25$ FFT grid, and therefore we can confirm its numerical accuracy.

Table 1. Comparison of Calculated Direct and Indirect Bandgaps of Diamond Based on GFT Methods and Experimental Data

bandgap	HF	SVWN	BLYP	B3LYP	exp
direct [eV]	14.6	5.9	5.7	7.4	7.3
indirect [eV]	12.6	4.2	4.4	6.0	5.48

The total energy per unit cell is obtained as follows.

$$E_{cell} = \sum_{\mathbf{Q}} Tr[\mathbf{D}(\mathbf{Q})\{\mathbf{T}(\mathbf{Q}) + \mathbf{V}_{ECP}(\mathbf{Q})\}] + \frac{2\pi}{N_{FT}^2 V_{cell}} \sum_{(\mathbf{G}\neq\mathbf{0})} \frac{|\rho^{valence}(\mathbf{G})|^2}{G^2} - \frac{4\pi}{N_{FT}} \sum_{A}^{cell} \sum_{(\mathbf{G}\neq\mathbf{0})} \frac{Z_A^{valence}\rho^{valence}(\mathbf{G})}{G^2} \exp(i\mathbf{G}\cdot\mathbf{R}_A) + \frac{2\pi}{V_{cell}} \sum_{A}^{cell}\sum_{A'}^{cell} \sum_{(\mathbf{G}\neq\mathbf{0})} \frac{Z_A^{valence} Z_{A'}^{valence}}{G^2} \exp\left(-\frac{G^2}{4\eta} + i\mathbf{G}\cdot\mathbf{R}_A\right) + \sum_{A}^{cell}\sum_{A'}^{cell} \sum_{(\mathbf{R}_A-\mathbf{R}_{A'}-\mathbf{Q}\neq\mathbf{0})} \frac{Z_A^{valence} Z_{A'}^{valence} erfc(\sqrt{\eta}|\mathbf{R}_A - \mathbf{R}_{A'} - \mathbf{Q}|)}{|\mathbf{R}_A - \mathbf{R}_{A'} - \mathbf{Q}|} - \left[\sum_{A}^{cell} (Z_A^{valence})^2\right]\sqrt{\frac{\eta}{\pi}} - \frac{1}{2}\left[\sum_{A}^{cell} Z_A^{valence}\right]^2 \frac{\pi}{\eta V_{cell}} + E_{XC} \quad (18)$$

Here, $\mathbf{G}$ is the reciprocal lattice vector. E_{XC} is the unit cell exchange-correlation energy, which is written as $E_{XC} = 0.5\sum_{\mathbf{Q}} Tr[\mathbf{D}(\mathbf{Q})\mathbf{V}_X^{Fock}(\mathbf{Q})]$ in the Hartree−Fock approximation. N_{FT} is the number of grids for the Fourier transform. In this paper, we adopt the Fast Fourier Transform (FFT) algorithm, and thus $\rho^{valence}(\mathbf{G}) = \sum_{\mathbf{r}_g} \rho^{valence}(\mathbf{r}_g) \exp(-i\mathbf{G}\cdot\mathbf{r}_g)$, where $\mathbf{r}_g$ is the grid point.

C. Recursion Relation. We discuss a technique for calculating eq (15-1). $V_{PE}(\mathbf{r})$ is expanded by plane waves by using the Fourier transform in the GFT method.

$$V_{PE}(\mathbf{r}) = \frac{1}{N_{FT}} \sum_{(\mathbf{G}\neq 0)} \frac{\upsilon_{PE}(\mathbf{G})}{G^2} \exp(i\mathbf{G}\cdot\mathbf{r}) \quad (19)$$

Here, $\upsilon_{PE}(\mathbf{G}) = 4\pi\sum_{\mathbf{r}_g} \rho_{Total}^{valence}(\mathbf{r}_g) \exp(-i\mathbf{G}\cdot\mathbf{r}_g)$ is the Fourier coefficient. Equation (15-1) can be rewritten using the Fourier coefficients as follows.

$$[\mathbf{V}_{Hartree}^{valence}(\mathbf{Q}) + \mathbf{V}_{LR-NA}^{valence}(\mathbf{Q})]_{\alpha\beta} = \frac{1}{N_{FT}} \sum_{(\mathbf{G}\neq 0)} \frac{\upsilon_{PE}(\mathbf{G})}{G^2} \langle \chi_\alpha^{\mathbf{0}} | \exp(i\mathbf{G}\cdot\mathbf{r}) | \chi_\beta^{\mathbf{Q}} \rangle \quad (20)$$

In order to calculate eq (20), we use the following recursion relation (cf. Appendix A).

$$\langle \mathbf{a} + \mathbf{1}_\xi | \exp(i\mathbf{G}\cdot\mathbf{r}) | \mathbf{b} \rangle = \left(P_\xi - R_\xi^A + \frac{iG_\xi}{2p}\right)\langle \mathbf{a} | \exp(i\mathbf{G}\cdot\mathbf{r}) | \mathbf{b} \rangle + \frac{1}{2p} N_\xi(\mathbf{a}) \langle \mathbf{a} - \mathbf{1}_\xi | \exp(i\mathbf{G}\cdot\mathbf{r}) | \mathbf{b} \rangle + \frac{1}{2p} N_\xi(\mathbf{b}) \langle \mathbf{a} | \exp(i\mathbf{G}\cdot\mathbf{r}) | \mathbf{b} - \mathbf{1}_\xi \rangle \quad (21\text{-}1)$$

$$\langle \mathbf{0} | \exp(i\mathbf{G}\cdot\mathbf{r}) | \mathbf{0} \rangle = \exp(-\mu|\mathbf{R}_A - \mathbf{R}_B|^2)\left(\frac{\pi}{p}\right)^{\frac{3}{2}} \times \exp\left(-\frac{G^2}{4p}\right)\exp(i\mathbf{G}\cdot\mathbf{P}) \quad (21\text{-}2)$$

$$|\mathbf{a}\rangle = (x - R_x^A)^{a_x}(y - R_y^A)^{a_y}(z - R_z^A)^{a_z} \exp(-g_a|\mathbf{r} - \mathbf{R}_A|^2) \quad (21\text{-}3)$$

$$p = g_a + g_b \quad (21\text{-}4)$$

$$\mu = \frac{g_a g_b}{g_a + g_b} \quad (21\text{-}5)$$

Here, $\mathbf{R}_A = (R_x^A R_y^A R_z^A)$, $\mathbf{a} = (a_x a_y a_z)$, $N_\xi(a) = a_\xi$, and $\mathbf{1}_\xi = (\delta_{x\xi}\delta_{y\xi}\delta_{z\xi})$ utilizing Kronecker's delta. $\mathbf{P} = (g_a\mathbf{R}_A + g_b\mathbf{R}_b)/(g_a + g_b)$. ξ represents one of x, y, or z. This recursion relation is an expansion of the Obara and Saika (OS) technique for atomic orbital (AO) integers. Note that the analytical technique based on this recursion relation provides highly efficient estimations for $\mathbf{V}_{Hartress}^{valence}(\mathbf{Q}) + \mathbf{V}_{LR-NA}^{valence}(\mathbf{Q})$.

We use the standard FFT algorithm, where the scaling is $O(N_{FT}\log N_{FT})$ and the scaling for atomic orbital integrations is $O(M^2 N_{FT})$ when we employ the above recursion relation. The fast multipole method (FFM) with a Gaussian basis set also yields a linear scaling estimation for the Hartree term.[5] In this respect, the GFT method may become an alternative for the FMM to calculate the Hartree term under the periodic boundary condtions. It should be noted that the GFT method cannot rigorously take into account isolated molecular systems because of the periodicity of plane wave.

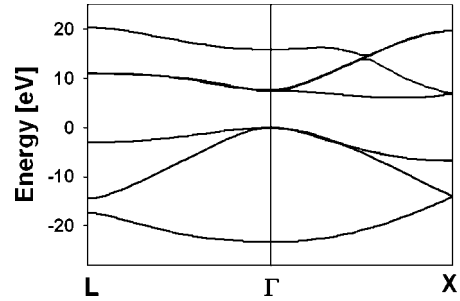

Figure 2. Energy band structure of diamond calculated by using the B3LYP functional.

III. Test Calculations

A. Diamond. In this section, we examine the energy band structure for a cubic bulk diamond on the basis of the GFT method. We have calculated the band energy by using the HF method and some DFT functionals. We employ three different types of DFT functionals such as the local density approximation (LDA), the generalized gradient approximation (GGA), and the hybrid functional. The Slater[29]-Vosko-Wilk-Nusair[30] (SVWN) and Becke[31,32]-Lee-Yang-Parr (BLYP) functionals are adopted for the LDA and the GGA calculations, respectively. We examine the B3LYP functional in the hybrid DFT method,[33] and we use the 6−21G* basis set proposed by Catti et al. for all calculations in this section.[34] Furthermore, we set the lattice constant to 3.57 Å and employ 25 × 25 × 25 k-points and 25 × 25 × 25 mesh grid points for the FFT procedure in order to calculate eq (20). We confirm the validity of the FFT grid size in Figure 1. We also checked the dependence of bandgap value on the truncation conditions. When we take into account the lattice integrals up to third neighboring cells, i.e. (7 × 7 × 7) cells, the value of the diamond's direct bandgap determined with the B3LYP functional is 7.35378 eV. On the other hand, a different truncation, which takes into account the second neighboring cells, yields 7.35358 eV. These calculated bandgap values are enough converged to discuss the property, and thus we employ the truncation condition of third neighboring cells in this paper. It should be noted that the "valence" Coulomb term in the GFT method is exactly determined because of the use of the Fourier transform. The truncation conditions affect only the Fock exchange and "core" Hartree terms.

Table 1 summarizes the direct and indirect (minimum) bandgaps determined by using the HF, SVWN, BLYP, and B3LYP methods. In this paper, the direct bandgap is defined as the eigenvalue energy difference between the top of the valence band and the bottom of the conduction band at $\mathbf{k} = 0$, and the indirect bandgap is the (minimum) energy difference between the top of the valence band and the bottom of the conduction band. We also show the corresponding values obtained from experiments in Table 1 and the B3LYP energy band structure in Figure 2. The SVWN functional underestimates the bandgaps in comparison with the experimental values, which is a well-known problem for LDA. There are no major differences between the LDA (SVWN) and GGA (BLYP) calculations. The GFT-SVWN method yields 5.5 eV for the direct bandgap and 4.2 eV for the indirect (minimum) bandgap. On the other hand, the direct and indirect bandgaps determined with the linear muffin-tin-orbital (LMTO) method are 5.7 and 4.1 eV, respectively.[35] The linear augmented plane wave (LAPW) method yields 5.6 and 4.0 eV for the direct and indirect bandgaps, respectively.[36] The plane-wave basis set calculation yields 5.57 and 3.90 eV for the same bandgaps.[37] From these calculations, we can confirm that the GFT-LDA method yields almost the same values with these calculations. On the other hand, the GFT-HF method overestimates the bandgap, yielding values for the direct and indirect bandgaps of 14.6 and 12.6 eV, respectively. On the other hand, the LMTO-HF method yields 14.6 eV for the direct bandgap and 12.6 eV for the indirect bandgap.[35] The LAPW-HF method yields 14.7 and 12.4 eV for the same values.[36]

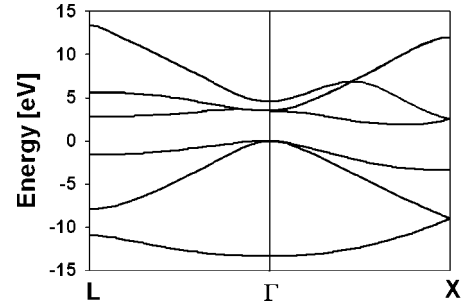

Figure 3. Energy band structure of silicon calculated by using the B3LYP functional.

Table 2. Exponents α (in a.u.) and the Coefficients *c* of the Gaussian Basis Set

	$\alpha_{s,p}$	c_s	c_p		α_d	c_d
			Si			
SP	1.10	−0.40	0.70	D	0.65	1.00
	0.30	1.00	1.00			
SP	0.18	1.00	1.00			
			Ga			
SP	0.90	−0.30	0.60	D	0.55	1.00
	0.19	−0.10	0.50			
SP	0.14	1.00	1.00			
			As			
SP	1.10	−0.40	0.70	D	0.65	1.00
	0.21	−0.20	0.50			
SP	0.18	1.00	1.00			

The B3LYP functional includes 80% of the Slater local density approximation $\mathbf{V}_X^{Slater}$ and 72% of the Becke88(B88)-type gradient correction $\Delta\mathbf{V}_X^{B88}$. In addition, 20% of the Fock exchange term is mixed into the functional. It was determined by Becke in 1993[33] that three parameters in the B3LYP functional reproduce the properties of molecules and the atoms of the G1 database.[38,39]

$$\mathbf{V}_{XC}^{B3LYP} = 0.8\mathbf{V}_X^{Slater} + 0.72\Delta\mathbf{V}_X^{B88} + 0.2\mathbf{V}_X^{Fock} + \mathbf{V}_C^{B3LYP} \tag{22-1}$$

$$\mathbf{V}_C^{B3LYP} = 0.19\mathbf{V}_C^{VWN} + 0.81\mathbf{V}_C^{LYP} \tag{22-2}$$

Here, $\mathbf{V}_C^{VWN}$ and $\mathbf{V}_C^{LYP}$ are the VWN and LYP correlation terms, respectively. There are only a few studies based on the B3LYP functional for crystalline systems. The direct and indirect bandgaps determined with the GFT-B3LYP method are 7.4 and 6.0 eV, respectively, while the crystal orbital (CO) method with the B3LYP functional yields 5.8 eV for the indirect bandgap.[40] In this regard, the B3LYP functional reproduces the experimental bandgap well. The nonlocal nature of the Fock exchange potential may be essential for reproducing the properties of semiconductors and insulators.

B. Silicon and GaAs. We show calculation results for silicon and GaAs in this section. We employ the effective core potential proposed by Labelo et. al for those calculations.[41,42] The exponents and the contraction coefficients of the atomic orbital for silicon, Ga, and As are summarized in Table 2. We employ 5.43 Å and 5.65 Å as the lattice constants for silicon and GaAs, respectively. The same values used in the previous section are adopted for other calculation parameters, such as k-point sampling and FFT-grid mesh grid points. Figures 3 and 4 show the energy band structure of silicon

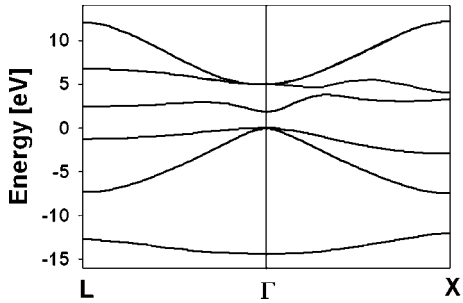

Figure 4. Energy band structure of GaAs calculated by using the B3LYP functional.

Table 3. Comparison of Calculated Direct and Indirect Bandgaps of Silicon Based on GFT Methods and Experimental Data

bandgap	HF	SVWN	BLYP	B3LYP	exp
direct [eV]	8.3	2.2	2.4	3.5	3.4
indirect [eV]	6.4	0.48	0.90	1.9	1.17

Table 4. Comparison of Calculated Direct Bandgap of GaAs Based on GFT Methods and Experimental Data

bandgap	HF	SVWN	BLYP	B3LYP	exp
direct [eV]	6.8	0.84	0.88	1.8	1.63

and GaAs, respectively. These figures are determined by the GFT-B3LYP method. We show the direct and indirect (minimum) bandgaps of silicon determined based on the HF, SVWN, BLYP, and B3LYP methods in Table 3. Table 3 also has experimentally obtained bandgaps. Similarly, we summarize the direct bandgap of GaAs in Table 4, where the direct bandgap of GaAs is the same with the minimum energy difference between the conduction and valence bands. The GFT-SVWN method yields 0.48 eV for the indirect bandgaps of silicon. In comparison, the plane wave (PW) basis set, the LMTO method, and the LAPW method yield 0.45 eV, 0.5 eV, and 0.5 eV for the property, respectively.[35−37] The GFT-HF method yields 6.4 eV for the indirect bandgap, and the LMTO and LAPW methods yield 5.6 and 6.3 eV for the property, respectively.[35,36] On the other hand, the direct bandgap of GaAs is determined as 0.84 eV based on the GFT-SVWN method, and the PW method and the LMTO method yield 0.67 eV and 0.83 eV for the same value, respectively.[43] The LDA(SVWN) and GGA(BLYP) methods underestimate the bandgaps, and the HF method overestimates the property. The tendency is the same current with the diamond's calculations. We also summarize the cohesive energies of silicon and GaAs determined with the SVWN, BLYP, B3LYP, HF methods in Table 5. The calculated values based on the DFT methods are close to the experimentally obtained cohesive energy. From these calculations, we conclude that the GFT method can yield results very similar to those of previous studies.

We have discussed only the B3LYP functional in this paper, but it should be noted that the HSE functional, which possesses a screened exchange term, was successfully applied to various systems.[13,44−47] In addition, Henderson et al. recently reported the middle-range Hartree−Fock-type exchange potential for the HISS functional.[48,49] The importance of the screened exchange term has been addressed through these studies. The screening effect on the exchange term may be essential to improve the description of the electronic structure of molecules and crystalline systems, and a discussion for the screening effect will be found in the literature.[50]

Table 5. Comparison of Calculated Cohesive Energy of Silicon and GaAs Based on GFT Methods and Experimental Data

cohesive energy [eV]	HF	SVWN	BLYP	B3LYP	exp
silicon	4.1	5.8	4.6	4.7	4.63
GaAs	3.1	6.8	4.2	4.5	6.52

VI. Summary

We have discussed the GFT method in relation to crystalline systems under the periodic boundary conditions, and applied this method to the energy band structure calculations for the diamond, silicon, and GaAs. The HF method overestimates the bandgap, while both the LDA(SVWN) and GGA(BLYP) methods underestimate it, although the B3LYP method reproduces the bandgap well in the case of diamond. The result indicates that the hybrid DFT methods, such as B3LYP, are useful for improving the molecular (material) properties of extended systems as well as isolated molecular systems. A discussion of the first-principle calculation studies for other materials on the basis of our technique will be provided elsewhere.

Acknowledgment. The authors would like to thank Prof. So Hirata of the University of Florida and Dr. Shoji Ishibashi of the National Institute of Advanced Industrial Science and Technology (AIST) for discussions on the DFT method.

Appendix A. Recursion Relation

In this Appendix, we derive the recursion relation of eq (22-1). The left term of eq (22-1) is expanded from the Gaussian product rule as follows.

$$\begin{aligned}\langle \mathbf{a}|\exp(i\mathbf{G}\cdot\mathbf{r})|\mathbf{b}\rangle &= \int\int\int (x-R_x^A)^{a_x}(y-R_y^A)^{a_y}(z-R_z^A)^{a_z}\times \\ &\exp(-g_a|\mathbf{r}-\mathbf{R}_A|^2)\times(x-R_x^B)^{b_x}(y-R_y^B)^{b_y}(z-R_z^B)^{b_z}\times \\ &\exp(-g_b|\mathbf{r}-\mathbf{R}_B|^2)\exp(i\mathbf{G}\cdot\mathbf{r})d\mathbf{r} = \exp(-\mu|\mathbf{R}_A-\mathbf{R}_B|^2)\times \\ &\int\int\int (x-R_x^A)^{a_x}(y-R_y^A)^{a_y}(z-R_z^A)^{a_z}(x-R_x^B)^{b_x}(y-R_y^B)^{b_y}\times \\ &(z-R_z^B)^{b_z}\exp(-p|\mathbf{r}-\mathbf{P}|^2)\exp(i\mathbf{G}\cdot\mathbf{r})d\mathbf{r} \\ &= \exp(-\mu|\mathbf{R}_A-\mathbf{R}_B|^2)I_xI_yI_z \quad \text{(A-1)}\end{aligned}$$

Here,

$$\begin{aligned}I_\xi(a_\xi,b_\xi) &= \int_{-\infty}^{\infty}(\xi-R_\xi^A)^{a_\xi}(\xi-R_\xi^B)^{b_\xi}\exp(-p(\xi-P_\xi)^2+iG_\xi\xi)d\xi \\ &= \sum_{\substack{m,n \\ m+n \text{ is even}}}\binom{a_\xi}{m}\binom{b_\xi}{n}\xi^{m+n}\pi\left(P_\xi-R_\xi^A+\frac{iG_\xi}{2p}\right)^{a_\xi-m}\times \\ &\left(P_\xi-R_\xi^B+\frac{iG_\xi}{2p}\right)^{b_\xi-n}(m+n-1)!!\times \\ &\sqrt{\pi/p}2^{-(m+n)/2}p^{-(m+n)}\exp\left(-\frac{G_\xi^2}{4p}+iG_\xi P_\xi\right) \\ &\equiv \sum_{\substack{m,n \\ m+n \text{ is even}}}\binom{a_\xi}{m}\binom{b_\xi}{n}L_\xi(a_\xi,b_\xi,m,n) \quad \text{(A-2)}\end{aligned}$$

In order to derive the recursion relation, we use the following first derivation of the equation.

$$\frac{1}{2g_a}\frac{\partial I_\xi(a_\xi,b_\xi)}{\partial R_\xi^A}=\frac{1}{2g_a}\sum_{\substack{m,n\\ m+n \text{ is even}}}\binom{a_\xi}{m}\binom{b_\xi}{n}L_\xi(a_\xi-1,b_\xi,m,n)\times$$
$$(a_\xi-m)\left(\frac{g_a}{p}-1\right)+\frac{1}{2g_a}\sum_{\substack{m,n\\ m+n \text{ is even}}}\binom{a_\xi}{m}\binom{b_\xi}{n}L_\xi(a_\xi,b_\xi-1,m,n)\times$$
$$(b_\xi-n)\frac{g_a}{p}+\frac{1}{2g_a}\frac{iG_\xi g_a}{p}I_\xi(a_\xi,b_\xi)$$
$$=a_\xi\left(\frac{1}{2p}-\frac{1}{2g_a}\right)I_\xi(a_\xi-1,b_\xi)+\frac{b_\xi}{2p}I_\xi(a_\xi,b_\xi-1)+\frac{iG_\xi}{2p}I_\xi(a_\xi,b_\xi) \quad \text{(A-3)}$$

Here, we used the following equation.

$$\binom{a_\xi}{m}(a_\xi-m)=\frac{a_\varsigma(a_\xi-1)\cdots(a_\xi-m+1)}{m(m-1)\cdots 1}(a_\xi-m)$$
$$=a_\xi\binom{a_\xi-1}{m} \quad \text{(A-4)}$$

We obtain the recursion relation from the above equations and $\partial|\mathbf{a}\rangle/\partial R_\xi^A=2g_a|\mathbf{a}+\mathbf{1}_\xi\rangle-N_\xi(\mathbf{a})|\mathbf{a}-\mathbf{1}_\xi\rangle$ as follows.

$$\langle\mathbf{a}+\mathbf{1}_\xi|\exp(i\mathbf{G}\cdot\mathbf{r})|\mathbf{b}\rangle=\frac{1}{2g_a}\frac{\partial}{\partial R_\xi^A}\langle\mathbf{a}|\exp(i\mathbf{G}\cdot\mathbf{r})|\mathbf{b}\rangle$$
$$+\frac{1}{2g_a}N_\xi(\mathbf{a})\langle\mathbf{a}-\mathbf{1}_\xi|\exp(i\mathbf{G}\cdot\mathbf{r})|\mathbf{b}\rangle$$
$$=\frac{-\mu}{g_a}(R_\xi^A-R_\xi^B)\langle\mathbf{a}|\exp(i\mathbf{G}\cdot\mathbf{r})|\mathbf{b}\rangle$$
$$+a_\xi\left(\frac{1}{2p}-\frac{1}{2g_a}\right)\langle\mathbf{a}-\mathbf{1}_\xi|\exp(i\mathbf{G}\cdot\mathbf{r})|\mathbf{b}\rangle+$$
$$\frac{b_\xi}{2p}\langle\mathbf{a}|\exp(i\mathbf{G}\cdot\mathbf{r})|\mathbf{b}-\mathbf{1}_\xi\rangle$$
$$+\frac{iG_\xi}{2p}\langle\mathbf{a}|\exp(i\mathbf{G}\cdot\mathbf{r})|\mathbf{b}\rangle+\frac{1}{2g_a}N_\xi(\mathbf{a})\langle\mathbf{a}-\mathbf{1}_\xi|\exp(i\mathbf{G}\cdot\mathbf{r})|\mathbf{b}\rangle$$
$$=\left(P_\xi-R_\xi^A+\frac{iG_\xi}{2p}\right)\langle\mathbf{a}|\exp(i\mathbf{G}\cdot\mathbf{r})|\mathbf{b}\rangle$$
$$+\frac{1}{2p}N_\xi(\mathbf{a})\langle\mathbf{a}-\mathbf{1}_\xi|\exp(i\mathbf{G}\cdot\mathbf{r})|\mathbf{b}\rangle+$$
$$\frac{1}{2p}N_\xi(\mathbf{b})\langle\mathbf{a}|\exp(i\mathbf{G}\cdot\mathbf{r})|\mathbf{b}-\mathbf{1}_\xi\rangle \quad \text{(A-5)}$$

Here, we used $-(R_\xi^A-R_\xi^B)(\mu/g_a)=P_\xi-R_\xi^A$.

References

(1) Pisani, C.; Dovesi, R.; Roetti, C. *Hartree-Fock Ab Initio Treatment of Crystallline Systems*; Springer-Verlag: Berlin, 1988; pp 32−46.

(2) Ladik, J. J. *Phys. Rep.* **1999**, *313*, 171.

(3) Hirata, S.; Iwata, S. *J. Chem. Phys.* **1997**, *107*, 10075.

(4) Hirata, S.; Head-Gordon, M.; Bartlett, R. J. *J. Chem. Phys.* **1999**, *111*, 10774.

(5) Kudin, K. N.; Scuseria, G. E. *Phys. Rev. B* **2000**, *61*, 16440.

(6) Ayala, P. Y.; Kudin, K. N.; Scuseria, G. E. *J. Phys. Chem.* **2001**, *115*, 9698.

(7) Izmaylov, A. F.; Scuseria, G. E.; Frisch, M. J. *J. Chem. Phys.* **2006**, *125*, 104103.

(8) Maschio, L.; Usvyat, D.; Manby, F. R.; Casassa, S.; Pisani, C.; Schutz, M. *Phy. Rev. B* **2007**, *76*, 075101.

(9) Izmaylov, A. F.; Scuseria, G. E. *Phys. Chem. Chem. Phys.* **2008**, *10*, 3421.

(10) Pisani, C.; Dovesi, R. *Int. J. Quantum Chem.* **1980**, *17*, 501.

(11) Delhalle, J.; Piela, L.; Bredas, J.-L.; Andre, J.-M. *Phys. Rev. B* **1980**, *22*, 6254.

(12) Helgaker, T.; Jorgensen, P.; Olsen, J. *Molecular Electronic-Structure Theory*; John Wiley & Sons, Ltd.: Chichester, 2000; pp 405−425.

(13) Krukau, A. V.; Vydrov, O. A.; Izmaylov, A. F.; Scuseria, G. E. *J. Chem. Phys.* **2006**, *125*, 224106.

(14) Izmaylov, A. F.; Scuseria, G. E. *J. Chem. Phys.* **2007**, *127*, 144106.

(15) Lippert, G.; Hutter, J.; Parrinello, M. *Mol. Phys.* **1997**, *92*, 477.

(16) Lippert, G.; Hutter, J.; Parrinello, M. *Theor. Chem. Acc.* **1999**, *103*, 124.

(17) Krack, M.; Parrinello, M. *Phys. Chem. Chem. Phys.* **2000**, *2*, 2105.

(18) VandeVondele, J.; Krack, M.; Mohamed, F.; Parrinello, M.; Chassaing, T.; Hutter, J. *Comput. Phys. Commun.* **2004**, *167*, 103.

(19) Füsti-Molnár, L.; Pulay, P. *J. Chem. Phys.* **2002**, *117*, 7827.

(20) Kurashige, Y.; Nakajima, T.; Hirao, K. *Chem. Phys. Lett.* **2006**, *417*, 241.

(21) Chen, X.; Langlois, J.-M.; Goddard, W. A., III *Phys. Rev. B* **1995**, *52*, 2348.

(22) Ordejon, P.; Artacho, E.; Soler, J. M. *Phys. Rev. B* **1996**, *53*, R10441.

(23) Delley, B. *J. Phys. Chem.* **1996**, *100*, 6107.

(24) Kurashige, Y.; Nakajima, T.; Hirao, K. *J. Chem. Phys.* **2007**, *126*, 144106.

(25) Wieferink, J.; Kruger, P.; Pollmann, J. *Phys. Rev. B* **2006**, *74*, 205311.

(26) Wieferink, J.; Kruger, P.; Pollmann, J. *Phys. Rev. B* **2007**, *75*, 153305.

(27) Baumeier, B.; Kruger, P.; Pollmann, J. *Phys. Rev. B* **2007**, 085407.

(28) Baumeier, B.; Kruger, P.; Pollmann, J. *Phys. Rev. B* **2007**, *76*, 205404.

(29) Slater, J. C. *Phys. Rev.* **1951**, *81*, 385.

(30) Vosko, S. H.; Wilk, L.; Nusair, M. *Can. J. Phys* **1980**, *58*, 1200.

(31) Becke, A. D. *Phys. Rev. A* **1988**, *38*, 3098.

(32) Lee, C.; Yang, W.; Parr, R. G. *Phys. Rev. B* **1988**, *37*, 785.

(33) Becke, A. D. *J. Chem. Phys.* **1993**, *98*, 5648.

(34) Catti, M.; Pavese, A.; Dovesi, R.; Saunders, V. R. *Phys. Rev. B* **1993**, *47*, 9189.

(35) Svane, A. *Phys. Rev. B* **1987**, *35*, 5496.

(36) Massidda, S.; Posternak, M.; Baldereschi, A. *Phys. Rev. B* **1993**, *48*, 5058.

(37) Godby, R. W.; Schluter, M.; Sham, L. J. *Phys. Rev. B* **1988**, *37*, 10159.

(38) Pople, J. A.; Head-Gordon, M.; Fox, D. J.; Raghavachari, K.; Curtiss, L. A. *J. Chem. Phys.* **1989**, *90*, 5622.

(39) Curtiss, L. A.; Jones, C.; Trucks, G. W.; Raghavachari, K.; Pople, J. A. *J. Chem. Phys.* **1990**, *93*, 2537.

(40) Muscat, J.; Wander, A.; Harrison, N. M. *Chem. Phys. Lett.* **2001**, *342*, 397.

(41) Stevens, W. J.; Basch, H.; Krauss, M. *J. Chem. Phys.* **1984**, *81*, 6026.

(42) Stevens, W. J.; Krauss, M.; Basch, H.; Jasien, P. G. *Can. J. Chem.* **1992**, *70*, 612.

(43) Agrawal, B. K.; Yadav, P. S.; Kumar, S.; Agrawal, S. *Phys. Rev. B* **1995**, *52*, 4896.

(44) Heyd, J.; Scuseria, G. E.; Ernzerhof, M. *J. Chem. Phys.* **2003**, *118*, 8207.

(45) Brothers, E. N.; Izmaylov, A. F.; Normand, J. O.; Barone, V.; Scuseria, G. E. *J. Chem. Phys.* **2008**, *129*, 011102.

(46) Heyd, J.; Peralta, J. E.; Scuseria, G. E.; Martin, R. L. *J. Chem. Phys.* **2005**, *123*, 174101.

(47) Vydrov, O. A.; Heyd, J.; Krukau, A. V.; Scuseria, G. E. *J. Chem. Phys.* **2006**, *125*, 074106.

(48) Henderson, T. M.; Izmaylov, A. F.; Scuseria, G. E.; Savin, A. *J. Chem. Phys.* **2007**, *127*, 221103.

(49) Henderson, T. M.; Izmaylov, A. F.; Scuseria, G. E.; Savin, A. *J. Chem. Theory Comput.* **2008**, *4*, 1254.

(50) Shimazaki, T.; Asai, Y. *Chem. Phys. Lett.* **2008**, *466*, 91.

CT800329M